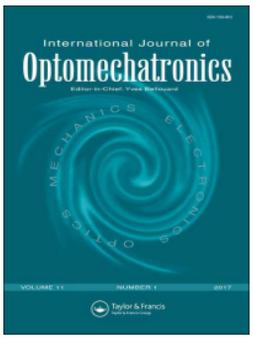

International Journal of Optomechatronics

ISSN: (Print) (Online) Journal homepage: https://www.tandfonline.com/loi/uopt20

Design of optical fiber Bragg grating-based sensors for flow measurement in pipes

Pedro Dieguez, Armando Rodriguez, Jose Carlos Urroz, Javier Lopez & Manuel Lopez-Amo

To cite this article: Pedro Dieguez, Armando Rodriguez, Jose Carlos Urroz, Javier Lopez & Manuel Lopez-Amo (2023) Design of optical fiber Bragg grating-based sensors for flow measurement in pipes, International Journal of Optomechatronics, 17:1, 2250444, DOI: 10.1080/15599612.2023.2250444

To link to this article: https://doi.org/10.1080/15599612.2023.2250444

Published online: 01 Sep 2023.

INTERNATIONAL JOURNAL OF OPTOMECHATRONICS
2023, VOL. 17, NO. 1, 2250444
https://doi.org/10.1080/15599612.2023.2250444

Design of optical fiber Bragg grating-based sensors for flow measurement in pipes

Pedro Dieguez[a,b], Armando Rodriguez[c,d], Jose Carlos Urroz[a,b], Javier Lopez[a,d], and Manuel Lopez-Amo[c,d]

[a]Engineering Department, Public University of Navarra, Pamplona, Spain; [b]School of Industrial and ICT Engineering, Public University of Navarra, Pamplona, Spain; [c]Electrical, Electronic and Communication Engineering Department, Public University of Navarra, Pamplona, Spain; [d]Institute of Smart Cities (ISC), Public University of Navarra, Pamplona, Spain

ABSTRACT

In this work, optical Fiber Bragg grating (FBG) sensors were used to measure water flow in pipes. Several types of coatings were incorporated into the design of the sensors to examine their effects on the elastic strain that the fiber underwent as a result of the water flow. ANSYS-CFX V2020 R2 software was used to model the elastic strain encountered by the fiber under various flow rates in order to assess the performance of the FBG sensors. The calculations and experimental data exhibited good convergence, demonstrating the accuracy of the FBG sensors in determining water flow. These calculations and procedures can be extrapolated to any other fluid.

KEYWORDS

Fiber Bragg grating; optical fiber sensor; coatings; Young's modulus; elastic strain measurement; flow measurement

1. Introduction

Optical fiber sensors based on Fiber Bragg Gratings (FBG) are probably the most successful optical fiber sensors. They consist of a periodic perturbation of the refractive index of the core of a fiber. This structure reflects a wavelength called the Bragg wavelength which depends on the separation of the maxima (or minima) of that perturbation. Because this separation can be tuned by using temperature or elastic strain variations, FGBs are suitable sensors for the measurement of elastic strain and temperature,[1] and indirectly, other parameters such as vibrations or humidity.[2] Several FBGs can be multiplexed into the same single-mode standard telecommunication fiber, and they have the big advantage that their information is coded into wavelength variations, being fairly immune to power fluctuations of the light source. It is important to remark that optical fibers are typically fabricated using silica, which is an insulating material well suited for underwater communications cables or underwater sensors such as hydrophones.[3]

In general, a distinction can be made between flowmeters based on the differential pressure principle (DP) and flowmeters based on new technologies (NTs). The first ones (DP), as the name suggests, cause a head loss in the flow, which can be accurately measured, and from this, the flow rate is derived. Some of the most commonly used are Venturi flowmeter, Pitot flowmeter, orifice plate flowmeter, and rotameter. These flowmeters are intrusive, causing effects of upstream conditions, and their accuracy is limited with an uncertainty of approximately 5%.[4,5]

CONTACT Armando Rodriguez armando.rodriguez@unavarra.es Electrical, Electronic and Communication Engineering Department, Public University of Navarra, Pamplona, Spain

Nomenclature

NT	new technologies	LPFBG	long-period fiber Bragg grating
FBG	fiber Bragg grating	PVC	polyvinyl chloride
DP	differential pressure	OSI	optical sensor interrogator
SMF	single-mode fiber	PC	personal computer

NT flowmeters (Coriolis, ultrasonic, vortex, electromagnetic, thermal, etc.) generally offer high accuracy, a wide range of flow rates, and nonintrusive flow measurement. However, each type has different limitations. A good and recent review of these sensors can be found in Ref.[6]

Three main sensing methods have been used for the development of optical fiber sensors for flow measurements: Intensity-modulated fiber sensors,[7] wavelength-modulated fiber sensors,[8] and distributed and phase-modulated optical fiber sensors.[9]

FBG sensors are probably the most utilized wavelength-modulated fiber sensors. We would like to remark on these recent publications of FBG sensors for flow measurements.

In Ref[10], an optical fiber anemometer based on Bragg grating inscribed in metal-filled microstructured optical fiber has been used for flow velocity measurement up to 2.5 m/s utilizing a LPFBG. In Ref[11–15], high-performance flow measurements using transversal FBGs to flow direction have been developed. The last sensor system incorporated 16 flow sensors measuring up to 2.5 m/s velocities.

Fiber optic flow sensors offer several advantages regarding the different types of flow measurement methods, including high accuracy, immunity to electromagnetic interference, and the ability to measure flow in harsh or hazardous environments due to the high chemical stability of silica. They can also be used to measure flow in opaque or nonconductive fluids, which is not possible with other flow measurement methods, such as electromagnetic flowmeters. These sensors do not need special calibration depending on the material used to fabricate the pipe, as happen with clamp-on ultrasonic flowmeters.[16] The cost varies depending on the type of flowmeter. In general, the more accurate and the larger the measurement range becomes, the more expensive the equipment is. A few years ago, fiber optic sensors and interrogation equipment were expensive, but prices have evolved downwards and have been reduced considerably, so that they are now competitive with other equipment. Therefore, it can be concluded that due to their simple structure, low cost and corrosion resistance, and fiber optic flow sensors have a promising future in next-generation industrial applications.[6]

Also, because the telecommunication cable used to connect these sensors is based on a very low attenuation material, remote measurement systems with a measurement range longer than 250 km can be deployed with or without optical amplification.[17,18]

In this work, we show how to design an optical fiber sensor based on FBGs with different coatings for measuring water flow in pipes. We start by giving a general outline of the mechanical behavior of FBG sensors in flow. Afterwards, we show the simulations carried out to choose the correct sensors design and their calibration and the difficulties in precisely monitoring waterflow rates. Finally, we review the results of our simulations and compare them with the experimental data obtained.

Thus, this work includes, for the first time to our knowledge, theoretical calculations, computational simulations, and laboratory tests to calibrate the elastic strain sensor based on FBGs within an optical fiber, in order to be used in flow measurements into pipes.

2. Sensor material analysis: Theory and computational simulation

The velocity of the water flowing through a pipe applies a hydrodynamic force on the fiber optic sensor wire, deforming, or simply stretching it. This deformation can be calculated theoretically

and computationally using flow dynamics, computational fluid dynamics, and structural simulation programs. In addition, this deformation can be experimentally measured by the sensor looking at changes in wavelength. The aim of this section is to calculate the unitary deformation of a wire, that includes an optical fiber sensor, using theoretical and computational methodologies. Also, to compare it with the deformations measured in the laboratory. These calculations help in the calibration of the sensors.

In the tests, a controlled and variable flow of water is passed through a transparent polyvinyl chloride (PVC) pipe of $67.8 \cdot 10^{-3}$ m inner diameter, and two sensor wires are placed perpendicular to the axis of the pipe. This wire is a FBG, with a silica diameter of 125 μm and a protecting acrylate coating of 250 μm (Figure 1) one sensor and the other sensor a protecting aluminum coating of 180 μm.

The colors represent the height of the different sections of the photographed fiber. Blue colors are associated with the lowest height. Therefore, it is the microscope table itself. Red ones correspond to the maximum height. It should be noted that our microscope (SENSOFAR Smart Neox electronic microscope, which uses a confocal technique) performs this level representation and also, we have used it to accurately measure the thickness of fiber and its coatings.

2.1. Flow dynamics calculations

The expression for the velocity of water flowing through the interior of a cylindrical pipe follows the well-known expression.[19]

$$\frac{V}{V_{\max}} = \left[1 - \left(\frac{r}{R}\right)\right]^{1/n} \tag{1}$$

where r is the radial distance, R the physical inner radius of the pipe, V the velocity corresponding to the radius r, V_{max} the maximum velocity (at the pipe axis) and n, an exponent obtained according to the experimental plot[19] which provides the n value as a function of the Reynolds' Number, R_e.[20]

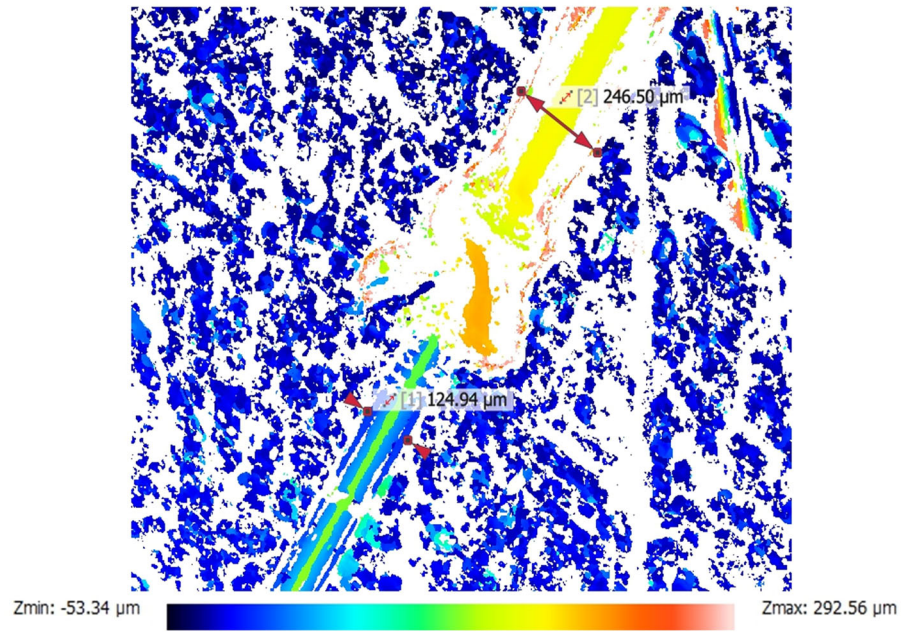

Figure 1. Microphotography of the fiber optic sensor taken with a SENSOFAR Smart Neox electronic microscope, using Confocal technique.

The average water velocity V_{ave} ($m{\cdot}s^{-1}$) in each section of the pipe is calculated from the equation

$$V_{ave} = (Q/3600)/S \tag{2}$$

where Q ($m^3{\cdot}h^{-1}$) corresponds to the tested flow rates and $S = 3.61 \cdot 10^{-3}$ m^2 the circular pipe section corresponding to an inner radius $R = 33.9{\cdot}10^{-3}$ m.

The Reynolds' Number formula is:

$$R_e = V_{\text{ave}} \cdot D \cdot \rho/\mu \tag{3}$$

where V_{ave} is the average velocity of the flow, ρ the density ($997\,kg{\cdot}m^{-3}$), and μ the dynamic viscosity of water at 282 °K and atmospheric pressure ($0.891 \cdot 10^{-3}$ $kg{\cdot}m^{-1}{\cdot}s^{-1}$).

The maximum velocity V_{max} is determined from the flow:

$$Q = \pi R^2 V_{ave} \;=\; \int_0^R V \; 2\pi r \; dr = 2\pi R^2 \int_0^R V_{\max}\left[1 - \left(\frac{r}{R}\right)\right]^{1/n}\left(\frac{r}{R}\right)\; d\left(\frac{r}{R}\right) \tag{4}$$

$$t = r/R \;\Rightarrow\; \pi R^2 V_{ave} \;=\; 2\pi R^2 V_{\max}\int_0^1 (1-t)^{1/n}\; tdt \;\Rightarrow\; V_{\max} = \frac{V_{ave}}{2\int_0^1 (1-t)^{1/n}\; tdt} \tag{5}$$

The integral is calculated according to the *beta* function:

$$\beta(x,y) = \int_0^1 (1-u)^{y-1}u^{x-1}du = \frac{\Gamma(x)\;\Gamma(y)}{\Gamma(x+y)} \tag{6}$$

Where

$$y - 1 = 1/n \;\Rightarrow\; y = 1 + 1/n \;;\; x = 2 \tag{7}$$

being *gamma* function:

$$\Gamma(z) = \int_0^\infty q^{z-1}e^{-q}dq \tag{8}$$

in the particular case, when $z \in \mathbb{N}$,

$$\Gamma(z) = (z-1)! \tag{9}$$

The expression of the maximum speed remains

$$V_{\max} = \frac{V_{ave}}{2}\;\frac{\Gamma\left(3+\frac{1}{n}\right)}{\Gamma\left(1+\frac{1}{n}\right)} \tag{10}$$

For the tested flow rate, the average and maximum velocities have been determined, so that from Equation (1) the velocity profile is obtained. Table 1 shows all flow parameter values measured and estimated according to the above equations for the tested rotational speed. Columns 1 and 2 show the rotational speed of the booster pump and the corresponding tested flow rates. Column 3 calculated values of mean water velocity Equation (2). Columns 4 and 5 show the Reynolds' Number Equation (3) and exponent n from reference.[21] Finally, column 6 shows the calculated values of maximum water velocity Equation (5).

The force exerted by a fluid stream on a long perpendicular cylinder (optical sensor's wire) is evaluated on the basis of the well-known fluid dynamics formula:

$$F = 0.5\;\rho\;C_d\;A\;V^2 \tag{11}$$

Table 1. Calculation of water flow parameters. RPM: tested rotational speed; Q: flow rates; V_{ave}: mean water velocity; R_e: Reynolds Number; n: exponent; V_{max}: maximum water velocity.

RPM	Q [$m^3 \cdot h^{-1}$]	V_{ave} [$m \cdot s^{-1}$]	R_e	n	V_{max} [$m \cdot s^{-1}$]
100	0.69	0.05	4028	5.30	0.07
200	6.43	0.49	37532	5.40	0.64
300	11.7	0.90	68294	5.52	1.16
400	16.6	1.28	96895	5.62	1.64
500	21.6	1.66	126081	5.73	2.12
600	26.4	2.03	154099	5.84	2.58
700	31.1	2.39	181533	5.94	3.03
800	35.5	2.73	207216	6.04	3.45
900	40.2	3.09	234650	6.14	3.89
1000	44.8	3.45	261501	6.24	4.32

Table 2. Calculation of force applied to the sensor at 700 RPM. r: distance from the pipe axis; V: flow velocity; R_e: Reynolds Number; C_d: drag coefficient; p: force per unit length; F: force applied.

	1	2	3	4	5	6	7	8	9	10
			Acrylate coated				Aluminum coated			
	r [m]	V [$m \cdot s^{-1}$]	R_e	C_d	p [$N \cdot m^{-1}$]	F[N]	R_e	C_d	p [$N \cdot m^{-1}$]	F[N]
1	0.0000	3.03	848	1.01	1.16	2.063E-03	610	1.08	0.89	1.588E-03
2	0.0018	3.00	840	1.02	1.15	2.043E-03	605	1.08	0.87	1.560E-03
3	0.0036	2.97	832	1.02	1.12	2.007E-03	599	1.08	0.86	1.530E-03
4	0.0054	2.94	824	1.02	1.10	1.966E-03	593	1.08	0.84	1.499E-03
5	0.0071	2.91	815	1.02	1.08	1.924E-03	587	1.08	0.82	1.468E-03
6	0.0089	2.88	805	1.02	1.05	1.880E-03	580	1.09	0.81	1.446E-03
7	0.0107	2.84	795	1.03	1.04	1.852E-03	573	1.09	0.79	1.411E-03
8	0.0125	2.81	785	1.03	1.01	1.802E-03	565	1.09	0.77	1.373E-03
9	0.0143	2.76	773	1.03	0.98	1.750E-03	557	1.09	0.75	1.338E-03
10	0.0161	2.72	761	1.03	0.95	1.698E-03	548	1.10	0.73	1.303E-03
11	0.0178	2.67	748	1.04	0.93	1.652E-03	538	1.10	0.71	1.258E-03
12	0.0196	2.62	733	1.04	0.89	1.588E-03	528	1.11	0.68	1.215E-03
13	0.0214	2.56	717	1.05	0.86	1.532E-03	516	1.11	0.65	1.166E-03
14	0.0232	2.50	698	1.05	0.82	1.455E-03	503	1.11	0.62	1.108E-03
15	0.0250	2.42	677	1.06	0.77	1.381E-03	488	1.12	0.59	1.051E-03
16	0.0268	2.33	652	1.07	0.72	1.290E-03	470	1.13	0.55	9.822E-04
17	0.0285	2.22	621	1.07	0.66	1.176E-03	447	1.13	0.50	8.929E-04
18	0.0303	2.07	580	1.09	0.58	1.043E-03	418	1.14	0.44	7.874E-04
19	0.0321	1.85	517	1.11	0.47	8.414E-04	372	1.16	0.35	6.331E-04

where F is the drag force, A is the projected area of the cylinder perpendicular to the direction of the velocity V of the stream, and C_d is the drag coefficient. This drag coefficient C_d, in the case of cylindrical bodies, is evaluated[21] as a function of the Reynolds' Number.

Considering the projected area of the cylinder $A = D \cdot L$ (diameter multiplied by cylinder length), the force p applied on the unit length of the cylinder can be determined by the expression :

$$p = 0.5 \ \rho \ C_d \ D \ V^2 \tag{12}$$

For each of the RPM or flow rate tested, the values of V, R_e, C_d, p, and F have been calculated for each of the radial coordinates considered, r. Table 2 shows, as an example, the values of these variables for 700 RPM or a flow rate of 31.1 $m^3 \cdot h^{-1}$. Twenty velocities corresponding to 20 values of the radius equally spaced every ($67.8 \cdot 10^{-3}/(2 \cdot 19)$) m have been obtained.

The velocity corresponding to the physical radius R is zero and does not appear in the table, due to the no-slip condition. Column 1 shows the radial coordinate r, where $r = 0$ m is the position of the pipe axis and $r = R = 33.9 \cdot 10^{-3}$ m is the coordinate corresponding to the pipe wall. Column 2 is the velocity V at that position.

Column 3 is the Reynolds Number, calculated with Equation (3) where the inside diameter of the pipe has been replaced by the outside diameter of the acrylate coating optical sensor's wire $D_w = 250$ μm and the average velocity V_{ave} by the velocity in column 2. Column 4 is the drag coefficient corresponding to the Reynolds Number in column 3, obtained from the experimental plot.[21] Column 5 is the force exerted per unit length of optical sensor's wire, obtained from Equation (12). Column 6 is the force applied on the radial coordinate r, obtained by multiplying column 5 by the distance corresponding to each coordinate $(R/19)$ m. Columns 7–10 are equivalent to columns 3–6 for the aluminum coating optical sensor's wire $D_w = 180$ μm. The only source of the differences between the two groups of columns is the different wire diameter, 250 μm vs 180 μm.

Figure 2 plots column 2 in the left y-axis and columns 7 and 10 in the right y-axis, column 1 in x-axis, from Table 2.

2.2. Structural computational simulation

The fiber deformations are calculated by computational simulation with ANSYS Mechanical APDL,[22] which is a finite element program that may be used to carry out static and dynamic structural analyses. LINK180 element type from ANSYS library is used. LINK180 is a 3D spar that is useful in a variety of engineering applications. That element can be used to model cables and wires. It is a uniaxial tension–compression element with three degrees of freedom at each node: translations in the nodal x, y, and z directions. Tension-only (cable) is supported.

This program is used to calculate the elastic strain on the sensor. Thus, the water force on the sensor (that is given in column 6 of Table 2 for coated acrylate sensor; or column 10 of the same Table for coated aluminum sensor, at position r of column 1) is the input, and the sensor elastic strain is the output. The wire stiffness calculation is obtained from the Young's modulus of the silica, $E = 72.045$ GPa for the coated acrylate sensor and $E = 68.672$ GPa for the coated aluminum

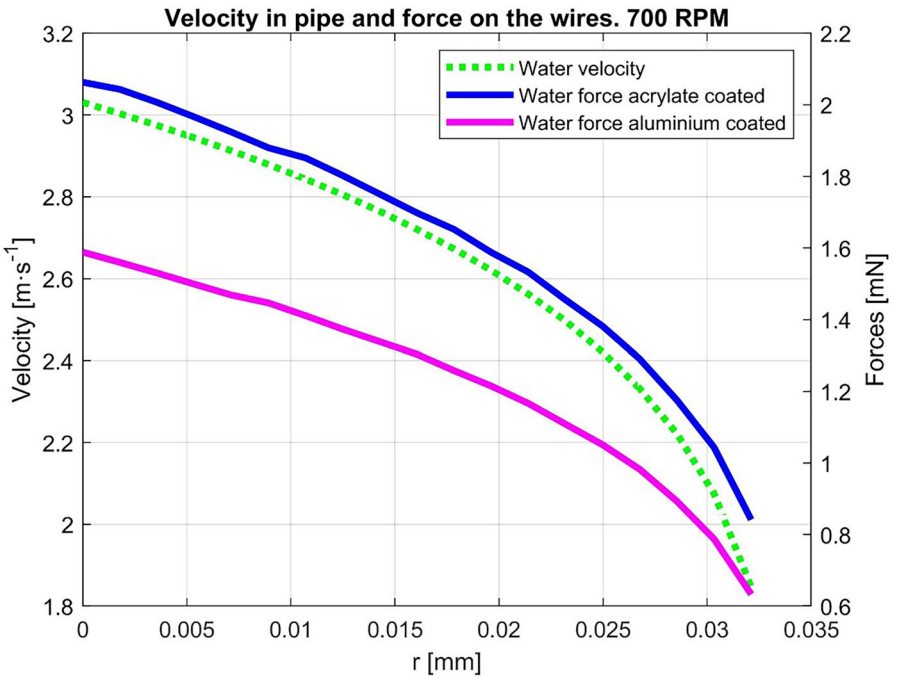

Figure 2. Calculated water velocity range in the pipe and forces applied on the optical sensors. r is the pipe's radial coordinate.

Table 3. Computational (C strain) and experimental (E strain) elastic strain.

RPM	100	200	300	400	500	600	700	800	900	1000
C Strain ($\mu\varepsilon$)	0	14	87	191	311	435	560	681	815	950
C Strain ($\mu\varepsilon$)	0	8	55	130	221	315	411	504	606	707
E Strain ($\mu\varepsilon$)	0	46	114	183	273	384	467	645	830	893
E Strain ($\mu\varepsilon$)	0	8	53	128	215	318	373	523	667	779

sensor. Both Young's Modulus values have been experimentally obtained (see next section). Our experimental data fits with previously published measurements of other researchers.[23] The stiffness of the acrylate is considered negligible because of its low Young's Modulus (less than 3 GPa). Although the stiffness of aluminum is high, it is considered negligible due to its lack of continuity. This is because the wire central area where the sensor is located is protected by acrylate and not by aluminum. The geometry of the silica part of the optical fiber sensor is a cylinder (diameter 125 μm). For symmetry, just half of the wire is considered, from its junction to the pipe to the pipe axis. As boundary conditions, zero displacements are imposed at the junction of the wire to the pipe and only longitudinal displacement along the axis of the pipe at the other end. The mesh of the half-wire has been made in such a way that there is a node at each position r of column 1 of Table 2. In addition, a pretension is considered, as discussed in the next section.

Twenty simulations were performed, one simulation for each 10 water flow rates,[24] for both coated sensor. The results of the elastic strain ε (without the initial elastic strain term due to pretension) multiplied by 10^6, to give the elastic strain in *microstrain* ($\mu\varepsilon$), are shown in Table 3, rows 2 and 3 for acrylate and aluminum-coated sensor, respectively. Row 1 of this Table 3 shows the same tested rotational speed of column 1 in Table 1.

3. Sensors' calibration

As previously stated, several optical fiber coatings were used during the validation of the optical fiber sensors. We tested classic coatings of acrylate as well as aluminum and PVC wrapping. This last one was employed in the form of a heat-shrinkable cap to increase the rigidity of the sensor and withstand high forces. The acrylate material utilized was the same as the common communications fiber. Aluminum alloy-coated optical fibers (from Technica) have been also tested in order to strengthen the system without compromising the fiber's flexibility.

The study is enhanced by the measurement of the real value in practice of the fiber optical elasticity coefficient. A set of calibrated weights was used for this purpose, and they were hanging on the fiber's tip to increase the amount of mass that was applied. The capacity to restore the initial conditions was tested multiple times with the suspended mass removed.

In order to calculate the deformation as a function of the mass straining the fiber, the initial value (at rest) of sensor's wavelength (λ_{FBG}) must be known. Considering the λ_{FBG} elastic strain sensitivity[1] as:

$$\Delta\lambda/\lambda = 0.79\ \Delta L/L \tag{13}$$

Figures 3 and 4 show the results of the characterization in the laboratory. Young's Modulus has been determined for sensors with the three different coatings under test. Figure 3 compares the wavelength shift that suffers the reflected Bragg grating wavelength of the sensors with two different coatings: acrylate and PVC, for different strains.

The strain was calibrated using different weights hung from each sensor, indicated in the horizontal axis of Figure 3. In this axis, there are also measurements interspersed without weight ("**No mass**") to see the recovery capacity of each sensor.

From this figure, it can be inferred that although acrylate protected sensor perfectly recovers its original value when the weight is removed, PVC coated sensor does not recover it completely. So that although PVC protects the sensor better than acrylate against particles suspended in

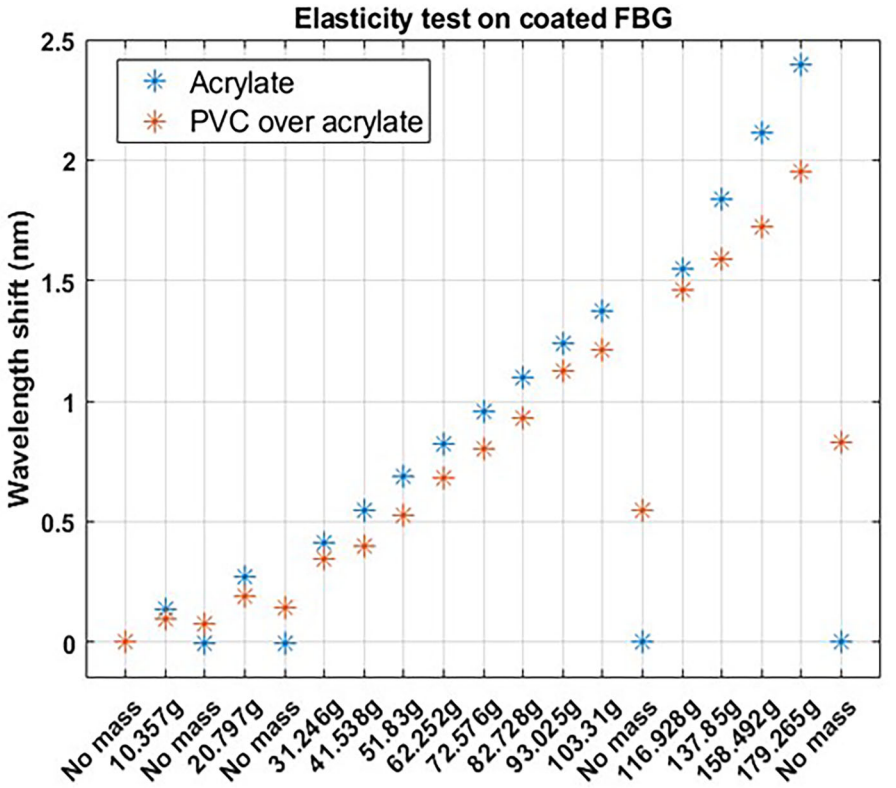

Figure 3. Elasticity test to both acrylate-coated and a fiber with a second layer of PVC. "No mass" means that the weight has been removed from the fiber.

liquids,[12] because this measured hysteresis, we decided to test another protecting coating. The selected protecting material for the new coating was aluminum.

In Figure 4, the stress test both for acrylate and aluminum coating is shown. With this experiment, Young's Modulus was experimentally measured for both coated sensors. For this test, the same weights used in Figure 3 were hung from the sensors and no hysteresis was detected for the aluminum-coated sensor.

4. Experimental results

The experiments were performed under constant temperature conditions, offsetting the sensitivity of the FBGs to this magnitude. In all scenarios, the Micron Optics® SM-130 Optical Sensor Interrogator was used and the sampling rate was set to 1 kHz—the highest it can afford—in order to acquire data from sensors. A custom-made software running on a PC allows to compute and carry out adequate statistical analysis to correctly establish a relationship between water flow rate and the elastic strain applied to the fiber.

4.1. Installation in pipes

The fluid dynamic study covered the pipe's dimensions, and a plastic union-shaped piece was designed to fit into the cross-section (Figure 5). The fibers were orthogonally placed on the holder with an epoxy resin seal to prevent water leakage. Both sensors were separated 65 mm from each other to avoid the turbulence associated with the "sail effect" within the water flow. Once the FBG is

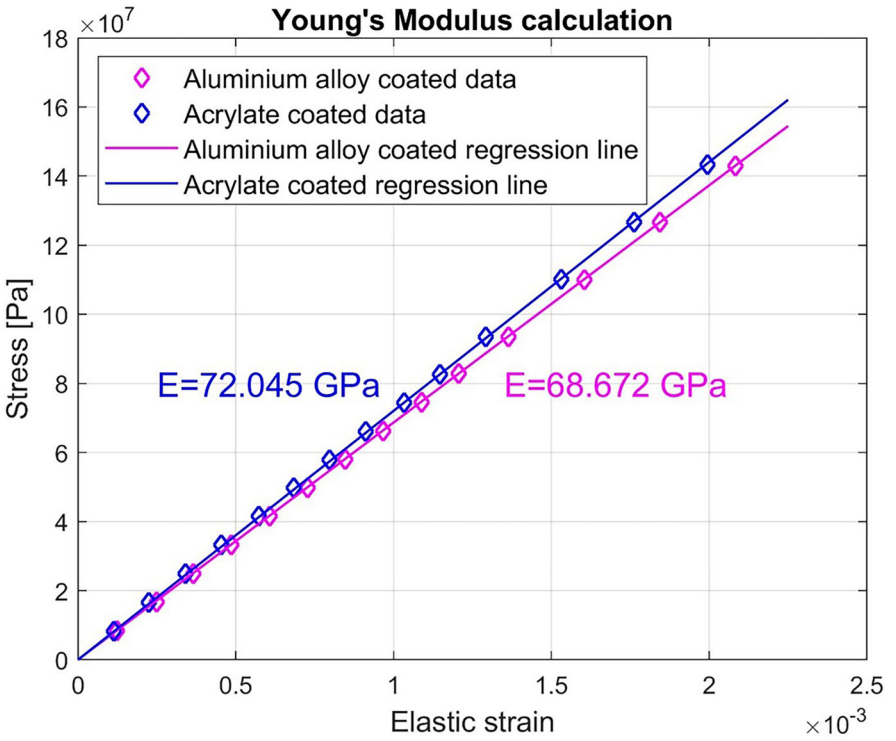

Figure 4. Young' Modulus of pure silica fiber coated with both acrylate and aluminum alloy.

Figure 5. (a) Pipe panel on which the experiment has been carried out; (b) mechanism for the installation of the sensors in the pipe; (c) Detail of the placement of the sensors in the support designed for the experiment.

prestressed,[9] hanging a weight of 19.5 g which implies a pretension of 15.6 MPa, both ends of the sensor are fixed to the inside of the pipe by means of a conventional glue.

The test measures the flow rate of the water flowing through the pipe and the deformation of the wire using an optical FBGs interrogator.

Using a hydraulic pump of brand *ITUR IN-50/250BF*, the test flow rate is ranged from 0.69 to 44.8 $m^3 \cdot h^{-1}$, according to Table 3. This flow rate is measured with a *ENDRESS + HAUSER PROMAG F* flow meter. After each modification of the flow rate, a time of approximately 60 s is waited in order to achieve a stabilized fluid and the corresponding flow rate reading. The experimental elastic strains are shown in rows 4 and 5, for acrylate and aluminum-coated sensor, respectively.

Figure 6 plots rows 2 and 4 in y-axis (calculated and experimental elastic strain of the acrylate-coated sensor), row 1 in x-axis, from Table 3 (calculated and experimental elastic strain of the aluminum-coated sensor). Besides, it depicts the plots of rows 3 and 5 in y-axis, row 1 in x-axis too, from same Table 3.

As it is shown in Figure 6, the theoretical and computational results correctly fit for low and high flow rates. The root mean square error for calculated and experimental data are 43.91 and 32.77 $\mu\varepsilon$ for acrylate and aluminum-coated sensor, respectively. These error values are relative because the same error at low water flow rates can be negligible at high flows. Nevertheless, there is a clear parallelism and a strong correlation between computational and experimental data. For the four data series, a parabolic fit $y = ax^2$ has been calculated, where y is the elastic strain and x the water flow rate. The utilized values for a coefficient were 0.5156 and 0.4879 $\mu\varepsilon \cdot m^{-3} \cdot h$, for computational data and test data, respectively, in case acrylate coated sensor. For the aluminum-coated sensor, a coefficient was 0.3811 and 0.4042, respectively.

These simulations allow us to predict the behavior of these kind of sensors in real applications and also, to correctly select the pre-stress[25] of these sensors for the estimated measurement range or to make temperature corrections.

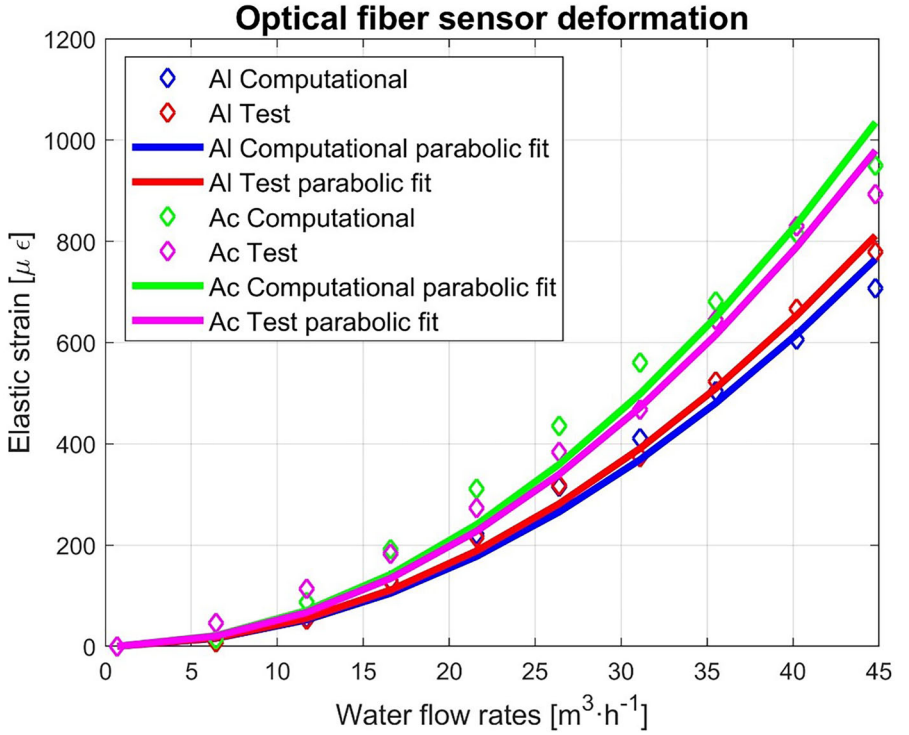

Figure 6. Computational versus measured elastic strain as function of the water flow rates for both acrylate (Ac) and aluminum (Al)-coated sensor.

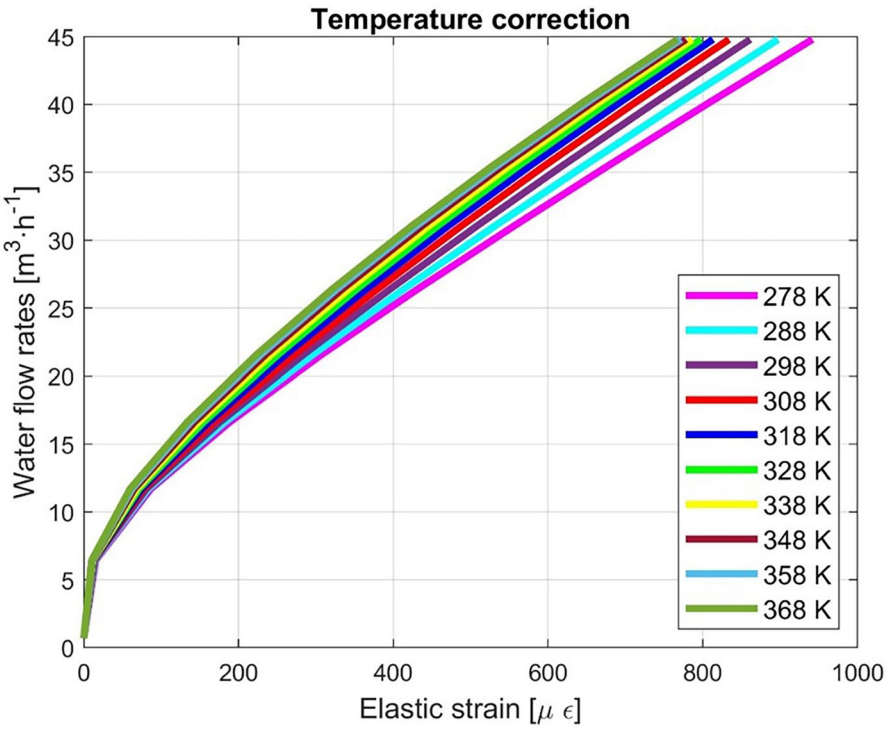

Figure 7. Computational water flow rates versus the elastic strain depending on temperature.

Table 4. *b* coefficient square root fit.

Temperature (K)	278	288	298	308	318	328	338	348	358	368
b coefficient [$m^3 \cdot h^{-1} \cdot \mu\varepsilon^{-0.5}$]	1.3611	1.3920	1.4219	1.4490	1.4728	1.4931	1.5103	1.5246	1.5366	1.5469

For example, since the objective of this work is the calculation of water flow rates based on the elastic strain, Figure 7 shows the water flow rates against the elastic strain for the acrylate-coated sensor; and the temperature influence in the measurement. For simplicity, in this simulation, we have ignored the coefficient of expansion of silica with temperature.

However, the elastic strain also depends on the temperature because both density and dynamic viscosity of the liquid depend on it. The plots clearly show the effect of increasing density with decreasing temperature. For these data series, a square root fit $y = b\sqrt{x}$ has been calculated, where y is the water flow rate and x the elastic strain. The values of coefficient b depending on temperature are shown in Table 4.

This work confirms the suitability of FBGs with different coatings for flow measurements in pipes. Depending on the on the type of liquid or the existence of suspended particles in the liquid, some coatings will be more suitable than others. With the model developed, it is possible to predict whether the sensitivity of the sensor is adequate for the range of measurements to be made.

5. Conclusions

FBG-based optical fiber sensors have proved to be an effective instrument for precise measurements of water flow.

This work demonstrates for the very first time to our knowledge, how to simulate the behavior of FBGs sensors inside water pipes for different water flow rates. The simulations can consider different coatings to protect the optical fiber sensors; and perfectly fits with experimental measurements. Previously, Young's Modulus of different coating for FBGs has been experimentally obtained. The findings of this study demonstrate that FBG sensors have great potential for measuring and analyzing fluid flow, and that aluminum, acrylate, and PVC coatings give valid alternative protections for practical applications.

This procedure is also valid for any other fluid by changing only two physical properties of the fluid: density and dynamic viscosity.

Funding

This work was supported in part by projects PID2019-107270RB-C02, funded by MCIN/AEI/10.13039/501100011033 and FEDER "A way to make Europe", and TED2021-130378B-C22 funded by MCIN/AEI/10.13039/501100011033 and European Union "Next generation EU"/PTR.

References

[1] Campanella, C.; Cuccovillo, A.; Campanella, C.; Yurt, A.; Passaro, V. Fibre Bragg grating based strain sensors: review of technology and applications. *Sensors (Basel)* **2018**, *18*, 3115. DOI: 10.3390/s18093115.

[2] Cusano A, Cutolo A, Albert J, eds. *Fiber Bragg Grating Sensors: Recent Advancements, Industrial Applications and Market Exploitation*. Bentham Science Publishers, 2011.

[3] Meng, Z.; Chen, W.; Wang, J.; Hu, X.; Chen, M.; Zhang, Y. Recent progress in fiber-optic hydrophones. *Photonic Sens.* **2021**, *11*, 109–122. DOI: 10.1007/s13320-021-0618-5.

[4] Suesser, M. Performance of classical Venturi tubes for application in cryogenic facilities. *AIP Conf. Proc.* 2012, *1434*, 1353–1362. DOI: 10.1063/1.4707061.

[5] Song, L.; Fang, F.; Zhao, J. Study on viscosity measurement using fiber Bragg Grating micro-vibration. *Meas. Sci. Technol.* **2013**, *24*, 015301. DOI: 10.1088/0957-0233/24/1/015301.

[6] Gupta, H.; Arumuru, V.; Jha, R. Industrial fluid flow measurement using optical fiber sensors: a review. *IEEE Sensors J.* **2021**, *21*, 7130–7144. DOI: 10.1109/JSEN.2020.3045506.

[7] Ang, J. L.; Idapalapati, S.; Asundi, A. K. Flow measurements using a simple fiber optic technique. *Proceedings of the 2012 World Congress on Advances in Civil, Environmental, and Materials Research (ACEM'12)* 2012, 2285–2296.

[8] Zamarreno, C. R.; Martelli, C.; Baroncini, V. H. V.; dos Santos, E. N.; da Silva, M. J.; Morales, R. E. M.; Zubiate, P.; Arregui, F. J.; Matias, I. R. Single and multiphase flow characterization by means of an optical fiber Bragg grating grid. *J. Lightwave Technol.* **2015**, *33*, 1857–1862. DOI: 10.1109/JLT.2015.2394788.

[9] Lipus, M. P.; Kranz, S.; Reinsch, T.; Cunow, C.; Henninges, J.; Reich, M. Distributed viscosity and flow velocity measurements using a fiber-optic shear stress sensor. *Sens. Actuators, A* **2022**, *345*, 113760. DOI: 10.1016/j.sna.2022.113760.

[10] Wang, J.; Liu, Z. Y.; Gao, S.; Zhang, A. P.; Shen, Y. H.; Tam, H. Y. Fiber-optic anemometer based on bragg grating inscribed in metal-filled microstructured optical fiber. *J. Lightwave Technol.* **2016**, *34*, 4884–4889. DOI: 10.1109/JLT.2016.2612299.

[11] Allil, A. S.; Dutra, F. D. S.; Dante, A.; Carvalho, C. C.; Allil, R.; Werneck, M. M. FBG-based sensor applied to flow rate measurements. *IEEE Trans. Instrum. Meas.* **2021**, *70*, 1–8. DOI: 10.1109/TIM.2020.3014751.

[12] Rodriguez-Rodriguez, A.; Urroz, J. C.; Dieguez, P. M.; Bravo, M.; Lopez-Amo, M.; Lopez, J. J. 2022 Development of a water flow and velocity optical fiber sensor for field testing. In *27th International Conference on* Optical Fiber Sensors. Optica Publishing Group:W4.5. DOI: 10.1364/OFS.2022.W4.5.

[13] Rodriguez Rodriguez, A.; Urroz, J. C.; Dieguez Elizondo, P.; Bravo Acha, M.; Lopez-Amo, M.; Lopez Rodriguez, J. J. Aluminum coated fiber optic sensor for enhancing flow rate measurement. In: Wuilpart M, Caucheteur C, eds. *European Workshop on Optical Fibre Sensors (EWOFS 2023)*. SPIE: Mons, Belgium; 2023. DOI: 10.1117/12.2678408.

[14] Liu, Z.; Wang, F.; Zhang, Y.; Jing, Z.; Peng, W. Low-power-consumption fiber-optic anemometer based on long-period grating with SWCNT coating. *IEEE Sensors J* **2019**, *19*, 2592–2597. DOI: 10.1109/JSEN.2019.2891044.

[15] Dzipalski, A.; Morton, J.; Papachristou, N.; Maier, R.; MacPherson, W.; Ristolainen, A.; et al. A multiplexed FBG-based sensor platform for flow and temperature measurements in the Baltic Sea. In: Wuilpart M,

Caucheteur C, eds. *European Workshop on Optical Fibre Sensors (EWOFS 2023)*. SPIE: Mons, Belgium; 2023, pp.108. DOI: 10.1117/12.2679756.

[16] Millan-Blasco, O.; Salazar, J.; Chavez, J. A.; Turo, A.; Garcia-Hernandez, M. J. 2017 Linearity error in Clamp-on ultrasonic flowmeters due to the installation on pipes made of dispersive materials. In 2017 IEEE International Instrumentation and Measurement Technology Conference (I2MTC). IEEE, pp.1–5. DOI: 10.1109/I2MTC.2017.7969959.

[17] Fernandez-Vallejo, M.; Rota-Rodrigo, S.; Lopez-Amo, M. Remote (250 km) Fiber Bragg grating multiplexing system. *Sensors (Basel)* **2011**, *11*, 8711–8720. DOI: 10.3390/s110908711.

[18] DeMiguel-Soto, V.; Leandro, D.; Lopez-Amo, M. Ultra-long (290 km) remote interrogation sensor network based on a random distributed feedback fiber laser. *Opt. Express* **2018**, *26*, 27189–27200. DOI: 10.1364/OE.26.027189.

[19] Power-law velocity profile - Turbulent Flow | nuclear-power.com. Nuclear Power. https://www.nuclear-power.com/nuclear-engineering/fluid-dynamics/turbulent-flow/power-law-velocity-profile-turbulent-flow/. Accessed May 16, 2023.

[20] Wieselsberger, C. NACA Technical Notes. Published online March 1922.

[21] Panton, R. L. *Incompressible flow*. 2nd ed. Wiley: New York; 1995.

[22] What is APDL? Ansys parametric design language. https://www.ansys.com/blog/what-is-apdl. Accessed May 16, 2023.

[23] Antunes, P.; Domingues, F.; Granada, M.; Andr, P. Mechanical properties of optical fibers. In: Yasin Moh, ed. *Selected topics on optical fiber technology*. InTech: Rijeka, Croatia; 2012.

[24] Tu, J.; Yeoh, G. H.; Liu, C. *Computational Fluid Dynamics: A Practical Approach*. Butterworth-Heinemann: Oxford, UK; 2018.

[25] Müller, M. S.; Hoffmann, L.; Buck, T. S.; Koch, A. W.; et al. 2008 Realization of a fiber-optic force-torque sensor with six degrees of freedom. In Otani Y, Bellouard Y, Wen JT, Hodko D, Katagiri Y, Kassegne SK, et al., eds. San Diego, CA, Nov. 2008, p. 72660S. DOI: 10.1117/12.807141.